

Transcending the MAX phases concept of nanolaminated early transition metal carbides/nitrides – the ZIA phases

M.A. Tunes^{a,*}, S.M. Drewry^{a,b}, F. Schmidt^{a,c}, J.A. Valdez^d, M.M. Schneider^a, C.A. Kohnert^a, T.A. Saleh^a, C.G. Schön^e, S. Fensin^d, O. El-Atwani^f, N. Goossens^g, S. Huang^g, J. Vleugels^g, S.A. Maloy^f, K. Lambrinou^{h,*}

^aMaterials Science and Technology Division, Los Alamos National Laboratory, United States of America

^bDepartment of Materials Science and Engineering, University of Tennessee, United States of America

^cDepartment of Nuclear Engineering, University of California Berkeley, United States of America

^dMaterials Physics and Applications Division, Los Alamos National Laboratory, United States of America

^eDepartment of Metallurgical and Materials Engineering, Universidade de São Paulo, Brazil

^fReactor Materials and Mechanical Design, Pacific Northwest National Laboratory, United States of America

^gDepartment of Materials Engineering, KU Leuven, Belgium

^hSchool of Computing and Engineering, University of Huddersfield, United Kingdom

Abstract

A new potential class of nanolaminated and structurally complex materials, herein conceived as the Zigzag Intermetallic (ZIA) phases, is proposed. A study of the constituent phases of a specific Nb–Si–Ni intermetallic alloy revealed that its ternary H-phase, *i.e.*, the Nb₃SiNi₂ intermetallic compound (IMC), is a crystalline solid with the close-packed *fcc* Bravais lattice, the 312 MAX phase stoichiometry and a layered atomic arrangement that may define an entire class of nanolaminated IMCs analogous to the nanolaminated ceramic compounds known today as the MAX phases. The electron microscopy investigation of the Nb₃SiNi₂ compound – the first candidate ZIA phase – revealed a remarkable structural complexity, as its ordered unit cell is made of 96 atoms. The ZIA phases extend the concept of nanolaminated crystalline solids well beyond the MAX phases family of early transition metal carbides/nitrides, most likely broadening the spectrum of achievable material properties into domains typically not covered by the MAX phases. Furthermore, this work uncovers that both families of nanolaminated crystalline solids, *i.e.*, the herein introduced *fcc* ZIA phases and all known variants of the *hcp* MAX phases, obey the same overarching stoichiometric rule $P_{x+y}A_xN_y$, where x and y are integers ranging from 1 to 6.

Keywords: MAX Phases, Electron Microscopy, Nanolaminated Crystalline Solids, ZIA Phases

*Corresponding authors:

Email addresses: m.a.tunes@physics.org (M.A. Tunes), k.lambrinou@hud.ac.uk (K. Lambrinou)

Special Dedication

This manuscript is dedicated to V. Nowotny, E. Reiffenstein, F. Benesovsky and W. Jeitschko of the University of Vienna, Austria, who first synthesized complex ternary carbides in the 1960/1970s, and to M.W. Barsoum of Drexel University, USA, who in the 1990/2000s revolutionized this field with his research on the MAX phases and the discovery of their 2D derivatives known as MXenes in 2011. Another dedication goes to E.I. Gladyshevskii, Yu.B. Kuz'ma and P.I. Kripyakevich of the Ivan Franko L'vovsk State University, former USSR, for their pioneering work on complex ternary intermetallics of the Nb_3Ni_2Si type in the 1960/1970s. The herein proposed "ZIA phases" are named after the ZIA indigenous nation of New Mexico, USA, where the Los Alamos National Laboratory is located.

1. Introduction

A revolution in materials science was undoubtedly achieved through the microstructural manipulation of materials on the nanoscale [1, 2]. When the dimensions of the building blocks of a material are confined in the 1-100 nm range, the material can be defined as nanostructured [3]. The nanoscale manipulation of matter through the engineering of structural modules, such as atomic clusters, precipitates, crystallites/grains, grain boundaries, molecules, and/or atomic layers has been an effective approach to achieve a set of extraordinary and unique properties in nanostructured materials, well beyond what is possible by conventional processing routes that target changes on the micro- and macroscale [1-4]. Transferring the superior properties of nanostructured materials to the bulk scale, a process demanding multiscale materials engineering, is one of the key challenges of contemporary materials science [4].

H. Gleiter – the scientist who introduced the term “nanostructured materials” [2] – predicted in 1992 [2] that this new research field would be significantly impacted by the emergence of two classes of nanostructured materials: ceramics and intermetallic phases. Gleiter’s prediction was partly realized in 1996 by M.W. Barsoum and his group, who made significant strides in the development and characterization of a class of nanolaminated ceramics with the $M_{n+1}AX_n$ general stoichiometry, where M is an early transition metal, A is an element mainly from groups 13-15 in the periodic table, X is C or N, and $n = 1, 2, \text{ or } 3$; these ceramic materials are known today as the MAX phases [5, 6]. The 1996 breakthrough by Barsoum and El-Raghy [5] consisted in the pioneering synthesis of quasi-phase-pure Ti_3SiC_2 via reactive hot pressing; notably, the existence of the Ti_3SiC_2 ternary carbide, which is the H-phase of the ternary Ti–Si–C system [7], had first been reported in 1967 by Jeitschko and Nowotny [8]. Starting by the successful synthesis and characterization of Ti_3SiC_2 , *i.e.*, the 312 ternary carbide of the Ti–Si–C system [7], Barsoum realized early in the 2000s that the Ti_3SiC_2 compound and other nanolaminated ternary carbides/nitrides form an entire new class of hexagonal close-packed (*hcp*) ceramics described by the $M_{n+1}AX_n$ strict stoichiometric rule and characterized by exceptional physicochemical and mechanical properties [6]. To date, around 155 ternary carbides/nitrides of early transition metals as well as numerous chemically complex solid solutions with the $M_{n+1}AX_n$ strict stoichiometry and precisely tailored properties have been experimentally synthesized [9, 10]. The exceptional properties of the MAX phases are attributed to their ordered *hcp* atomic arrangement of M_6X ceramic-like octahedra and intercalated A metallic-like layers, which results in nanolaminated unit cells with long-range translational symmetry. Since their inception, the MAX phases [11, 12] and their 2D derivatives known as MXenes [13-17] have been proposed for various applications in diverse industrial/technological fields, including energy

storage, fuel cells, biomedical, photonics/phononics [18–30], as well as in advanced nuclear fusion and fission reactor systems [31–42].

This work focuses on a single member of a potential class of nanolaminated intermetallic compounds (IMCs), herein named the “zigzag intermetallic” phases or simply the ZIA phases. The first candidate ZIA phase introduced in this work is the Nb_3SiNi_2 ternary IMC, which is considered the H-phase of the Nb–Si–Ni system [43–46]. This work reports the experimental synthesis of quasi-phase-pure Nb_3SiNi_2 via reactive hot pressing and also addresses, for the first time, the aspects of crystal structure nanolamination and ‘zigzag’ atomic arrangement in the Nb_3SiNi_2 IMC. At first glance, the ZIA phases share many similarities with the MAX phases, such as crystal structure nanolamination and obeying the $\text{M}_{n+1}\text{AX}_n$ stoichiometric rule with $n = 2$; however, their true potential cannot yet be reliably assessed due to the scarcity of available data. We believe that the nanolaminated ZIA phases and their possible 2D derivatives might have a potential commensurate with that of the nanolaminated MAX phases and their 2D derivatives known as MXenes. In case future research validates this hypothesis, then a whole new research field will have been inaugurated and the prediction of Gleiter [1, 2] on the existence of ‘nanostructured IMCs’ will have come true, at the same time.

2. Results and discussion

2.1. Synthesis of phase-pure Nb_3SiNi_2

Initially, arc melting was employed to produce bulk materials made of the Nb_3SiNi_2 IMC ZIA phase. The microstructure of the as-cast Nb–Si–Ni intermetallic alloy was first studied by SEM with the aid of a backscattered electron (BSE) detector. The compositional contrast of the BSE image in Fig. 1A indicates the presence of four distinct phases in the as-cast alloy microstructure, a finding supported by both EDX elemental mapping and XRD. Phase identification by XRD (Fig. 1C) revealed the (metastable) co-existence of the Nb_3SiNi_2 H-phase (candidate ZIA phase), the Nb_7Ni_6 μ -phase, the Ni_3SiNb_2 ternary Laves (L) phase and the Nb_4NiSi T-phase. These four phases were peak-indexed in accordance with data provided by the ICSD database [47] and were also identified as possible phases during the experimental investigation of phase equilibria in the Nb–Si–Ni refractory alloy system [46]. The nominal stoichiometries and measured EDX elemental compositions of the four phases in the as-cast alloy are provided in Table 1, showing that all phases formed as imperfect (off-stoichiometric) solid solutions during melt solidification rather than as stoichiometric compounds. The formation of solid solutions in the Nb–Si–Ni system has been previously reported by dos Santos *et al.* [46]; a strong indication of solid solution formation is encountered in the dissolution of significant amounts of Si in the Nb_7Ni_6 μ -phase, as previously reported [46] and also seen in Table 1. Even though arc-melting targeted the formation of bulk materials (discs) made primarily of the Nb_3SiNi_2 IMC ZIA phase, the presence of four distinct phases in the as-cast alloy microstructure is a clear violation of the Gibbs’ phase rule for a ternary alloy [48], indicating that thermodynamic equilibrium has not been reached via arc melting synthesis. This is most likely caused by the loss of substantial amounts of Ni, which is volatile in vacuum above its melting point (1728 K). By looking at the CALPHAD phase equilibria calculated in this work (Fig. 2C) in conjunction with the microstructure of the as-cast alloy (Fig. 1A), it is reasonable to assume that the (rapid) solidification of the melt produced solid solutions of three main phases, *i.e.*, the Nb_3SiNi_2 H-phase, the Nb_7Ni_6

Table 1: Nominal stoichiometries vs. actual compositions of the phases identified by SEM/EDS in the arc-melted (as-cast & annealed) and RHP Nb–Si–Ni intermetallic alloy samples.

Arc-Melted Nb–Si–Ni Alloy Samples					
Phases Identified		Stoichiometry	Nb [at.%]	Si [at.%]	Ni [at.%]
H-phase (as-cast)		Nb ₃ SiNi ₂ (ZIA phase)	46.5±3.2	18.4±4.0	35.1±1.9
H-phase (annealed)			46.4±3.0	18.6±3.7	35.0±1.5
H-phase (expected)			50.0	17.0	33.0
Laves phase (as-cast)		Ni ₃ SiNb ₂	31.9±2.7	21.8±3.5	46.3±1.8
Laves phase (annealed)			31.3±2.4	20.1±3.1	48.6±1.2
Laves phase (expected)			33.0	17.0	50.0
μ -phase (as-cast)		Nb ₇ Ni ₆ *	45.2±3.1	13.5±3.8	41.3±1.9
μ -phase (annealed)			43.8±3.0	13.5±3.7	42.7±1.5
μ -phase (expected)			53.8	-	46.2
T-phase (as-cast)		Nb ₄ NiSi	62.8±3.8	25.8±4.7	11.4±2.5
T-phase (annealed)			62.6±3.8	25.3±4.7	12.0±1.9
T-phase (expected)			66.0	17.0	17.0
RHP Nb–Si–Ni Alloy Samples					
Sintering T [K]	Phases Identified	Nb [at.%]	Si [at.%]	Ni [at.%]	O [at.%]
1523	H-Nb ₃ SiNi ₂	53.86±0.16	12.71±0.03	33.43±0.12	-
	L-Ni ₃ SiNb ₂	38.60±0.12	17.63±0.03	43.77±0.12	-
	μ -Nb ₇ Ni ₆	71.99±0.13	17.17±0.03	10.85±0.07	-
1623	H-Nb ₃ SiNi ₂	53.57±0.15	13.26±0.03	33.17±0.12	-
	L-Ni ₃ SiNb ₂	36.25±0.15	17.49±0.04	46.27±0.16	-
	μ -Nb ₇ Ni ₆	-	-	-	-
1723	H-Nb ₃ SiNi ₂	52.80±0.17	13.12±0.04	34.08±0.14	-
	L-Ni ₃ SiNb ₂	36.32±0.11	17.47±0.03	46.21±0.11	-
	μ -Nb ₇ Ni ₆	65.96±0.21	8.43±0.04	4.65±0.09	20.96±0.05

* Si has been reported to dissolve in the binary Nb₇Ni₆ IMC, forming μ -phase solid solutions [46].

μ -phase and the Ni₃SiNb₂ L-phase, while the Ni-impoverished residual melt formed the Nb₄NiSi T-phase (see the 1423 K isotherm in Fig. 2C). This hypothesis is supported by the small fraction of the Nb₄NiSi T-phase in the as-cast alloy (Fig. 1A).

The homogenization annealing at 1421 K was performed, first and foremost, to investigate whether the four-phase assembly of the as-cast Nb–Si–Ni intermetallic alloy would converge to an alloy with a higher fraction of the Nb₃SiNi₂ IMC ZIA phase. The annealing aimed also at a first assessment of the thermal stability of the Nb₃SiNi₂ ZIA phase of interest in this work. The SEM/EDS/XRD analysis of the annealed alloy (Figs. 1B & 1C) showed that it still consisted of the same four phases with a slightly increased fraction of the Nb₃SiNi₂ H-phase that appears able to sustain these conditions; the increase of the latter was not sufficient to suggest that the selected annealing conditions were capable of transforming the phase assembly of the as-cast alloy into an alloy primarily composed of the Nb₃SiNi₂ IMC. This suggests that solid-state diffusion at 1421 K is relative slow, and that annealing treatments much longer than 336 h would be required to achieve alloy homogenization at 1421 K; moreover, the fact that the alloy composition after solidification of the melt appears to be off the Nb₃SiNi₂ stoichiometry (primarily due to the loss of Ni) will prevent the formation of a phase-pure Nb₃SiNi₂ material, irrespective of the annealing duration and temperature. Fig. 1B reveals that the microstructure of the annealed alloy

was slightly modified, suggesting limited coarsening and change of grain morphology (e.g., the Nb₇Ni₆ μ -phase grains appear more angular and equiaxed in the annealed alloy than in the as-cast alloy). The limited microstructural changes indicate that the thermodynamically metastable as-cast alloy strives to achieve equilibrium during isothermal annealing, forming more Nb₃SiNi₂ and transitioning towards a slightly coarser microstructure, however, the imposed annealing conditions are not conducive to achieving equilibrium. The elemental compositions of the four phases in the annealed alloy, as determined by EDX analysis, are provided in Table 1. Additional BSE images of the microstructures of both as-cast and annealed arc-melted samples are given in Fig. S1 (Supplementary Information). The unsuccessful attempt to synthesize phase-pure Nb₃SiNi₂ via arc melting showed that this processing route is difficult to master, mainly due to the poorly controlled losses of the constituting elements above their melting points (e.g., $T_m(\text{Ni}) = 1728 \text{ K}$, $T_m(\text{Nb}) = 2750 \text{ K}$, $T_m(\text{Si}) = 1683 \text{ K}$). Moreover, it became clear that it is necessary to calculate the equilibrium phase mixtures at the annealing temperature (1421 K) and at higher temperatures (in order to understand melt solidification), as prior studies have only examined the 1073, 1323 and 1473 K isotherms of the Nb–Si–Ni system [43–46].

The results of this work contradict the early work of Gladyshevskii *et al.* [43], who reported that by melting a feedstock of elemental powders under an inert gas atmosphere (presumably, argon), they were able to produce quasi-phase-pure Nb₃SiNi₂ with only a small amount of a ternary Laves phase (presumably, the Ni₃SiNb₂ ternary IMC also detected in this work). These authors used light optical microscopy to confirm the phase purity of their arc-melted alloys, and powder XRD to propose the existence of a group of (atomically ordered) ternary IMCs with the H-phase structure (space group $Fd\bar{3}m$) and the R₃SiNi₂ general stoichiometry, with R being the early transition metals Mn, Cr, V, Nb and Ta [43]. Apart from demonstrating a much better command of the arc-melting processing route, the 1964 pioneering work by Gladyshevskii *et al.* [43] paved the way for the study of the ZIA phases proposed in this work. In a similar manner, the 1967 work by Jeitschko *et al.* [7] opened the way for the further development of the class of early transition metal ternary carbides/nitrides known as the MAX phases almost 40 years later by Barsoum *et al.* [5, 6].

A thorough thermodynamic assessment of the Nb–Si–Ni system was only recently conducted – 50 years after Gladyshevskii’s pioneering work – in a set of works published by dos Santos *et al.* [44–46]. In an attempt to reproduce the results of Gladyshevskii *et al.* [43], dos Santos *et al.* [45] synthesized 12 different alloy compositions in the Nb–Si–Ni system via arc melting and subsequently homogenized the as-cast samples at 1073 K for longer times (1000 h). Curiously, the Nb₃SiNi₂ phase was not found in any of the 12 homogenized samples characterized by means of SEM/EDX and XRD. It is presently not understood whether the difference in atmosphere during melting – reducing (H₂) in Gladyshevskii *et al.* [43] and possibly slightly oxidizing (argon, Ar, of unknown purity) in dos Santos *et al.* [44–46] – is accountable for the difference in the produced arc-melted alloys. Based on their data, dos Santos *et al.* suggested a homogenization isothermal annealing at higher temperatures to explore the thermodynamic equilibrium in this system [45]. In a more extensive follow-up study, dos Santos *et al.* investigated 48 alloy compositions in the Nb–Si–Ni system, implementing two different heat treatment approaches: (a) 1323 K for 336 h and (b) 1473 K for 504 h [46]. Using SEM/EDX and XRD after homogenization annealing, the Nb₃SiNi₂ phase was only observed in seven samples, but none of these were phase-pure Nb₃SiNi₂.

All 7 samples exhibited triphasic microstructures, each comprising two or three of the four principal phases, *i.e.*, the ternary Laves, μ , T- and H-phases; small fractions of the NbNi_3 IMC or the unknown Z phase were also reported in 3 of the 7 samples. The Z phase is one of three phases with unresolved crystal structure – tentatively designated X, Y and Z – found by dos Santos *et al.* after annealing select Nb-Si-Ni alloy compositions at 1473 K for 504 h [46].

Careful consideration of both the prior attempts by dos Santos *et al.* [45, 46] and the outcome of this work demonstrated that the synthesis of phase-pure Nb_3SiNi_2 via arc melting is challenging. Even though Gladyshevskii *et al.* [43] reported that the production of quasi-phase-pure Nb_3SiNi_2 is possible via the melting of an elemental powder feedstock with identical composition in an inert gas atmosphere, high-vacuum plasma arc melting methods have been empirically known to face challenges during the synthesis of compounds with strict stoichiometries, such as the ternary IMCs designated as the ZIA phases in this work, or the ternary carbides/nitrides known as the MAX phases [49]. As already mentioned, one important challenge is the evaporation of alloying elements in the vacuum chamber [50]. Given the strict stoichiometry of the ZIA phases and the 312 MAX phases, the processing route as well as the starting powder feedstock must be always carefully adjusted to produce materials with high phase purity. For example, Goossens *et al.* [51] explained rather recently why the use of early transition metal hydride powders produces MAX phase-based ceramics with higher phase purities than the use of elemental starting powders. These authors proved that the use of metal hydride powders lowers the formation temperature of MAX phase precursor phases (*e.g.*, binary IMCs), increases the formation temperature of competing phases (*e.g.*, binary carbides), and suppresses the oxidation of oxidation-prone powders (*e.g.*, Zr) by providing a reducing (H_2 -rich) atmosphere caused by powder dehydrogenation, thus allowing the use of finer powder feedstocks. Based on the above, it was decided in this work to employ reactive hot pressing (RHP) of carefully adjusted powder feedstocks consisting of hydride ($\text{NbH}_{0.89}$) and elemental powders (Ni & Si) to produce phase-pure Nb_3SiNi_2 . The synthesis efforts proved to be successful at three different sintering temperatures (*i.e.*, 1523 K, 1623 K, and 1723 K), producing quasi-phase-pure Nb_3SiNi_2 with a small fraction of the ternary Ni_3SiNb_2 Laves phase, and tiny amounts of oxidic inclusions (NbO & NiO), presumably stemming from the limited oxidation of the raw powders. BSE images of the microstructures and WDXS elemental maps of all quasi-phase-pure Nb_3SiNi_2 materials are shown in Fig. 2B, next to their XRD patterns (Fig. 2A). Additional BSE micrographs and EDS elemental maps of all RHP alloy samples are shown in Fig. S2 (Supplementary Information).

The results of CALPHAD calculations of the phase equilibria in the ternary Nb–Si–Ni system at 1423 K (*i.e.*, close to the temperature of isothermal annealing, 1421 K, of the arc-melted alloy), 1523 K, 1623 K and 1723 K are shown in Fig. 2C. These calculations suggest that melt solidification during vacuum arc melting produced mainly a ternary phase mixture comprising the L- Ni_3SiNb_2 line compound, the H- Nb_3SiNi_2 point compound (targeted ZIA phase), and the μ - Nb_7Ni_6 phase-field compound with enhanced Si solid solubility. Due to the anticipated loss of Ni during vacuum arc melting, a small fraction of the melt was Ni-poor and solidified as the T- Nb_4SiNi point compound, which appears only in the 1423 K isotherm (Fig. 2C). On the other hand, all three alloys synthesized via RHP at 1523/1623/1723 K resulted in quasi-binary phase mixtures made of the H- Nb_3SiNi_2 (targeted ZIA phase) and L- Ni_3SiNb_2 compounds. The NbO and NiO oxide impurities present in the RHP alloys are not encountered in the arc-melted alloys due

to the much higher processing temperatures associated with the complete melting of all raw elemental powders during arc melting synthesis.

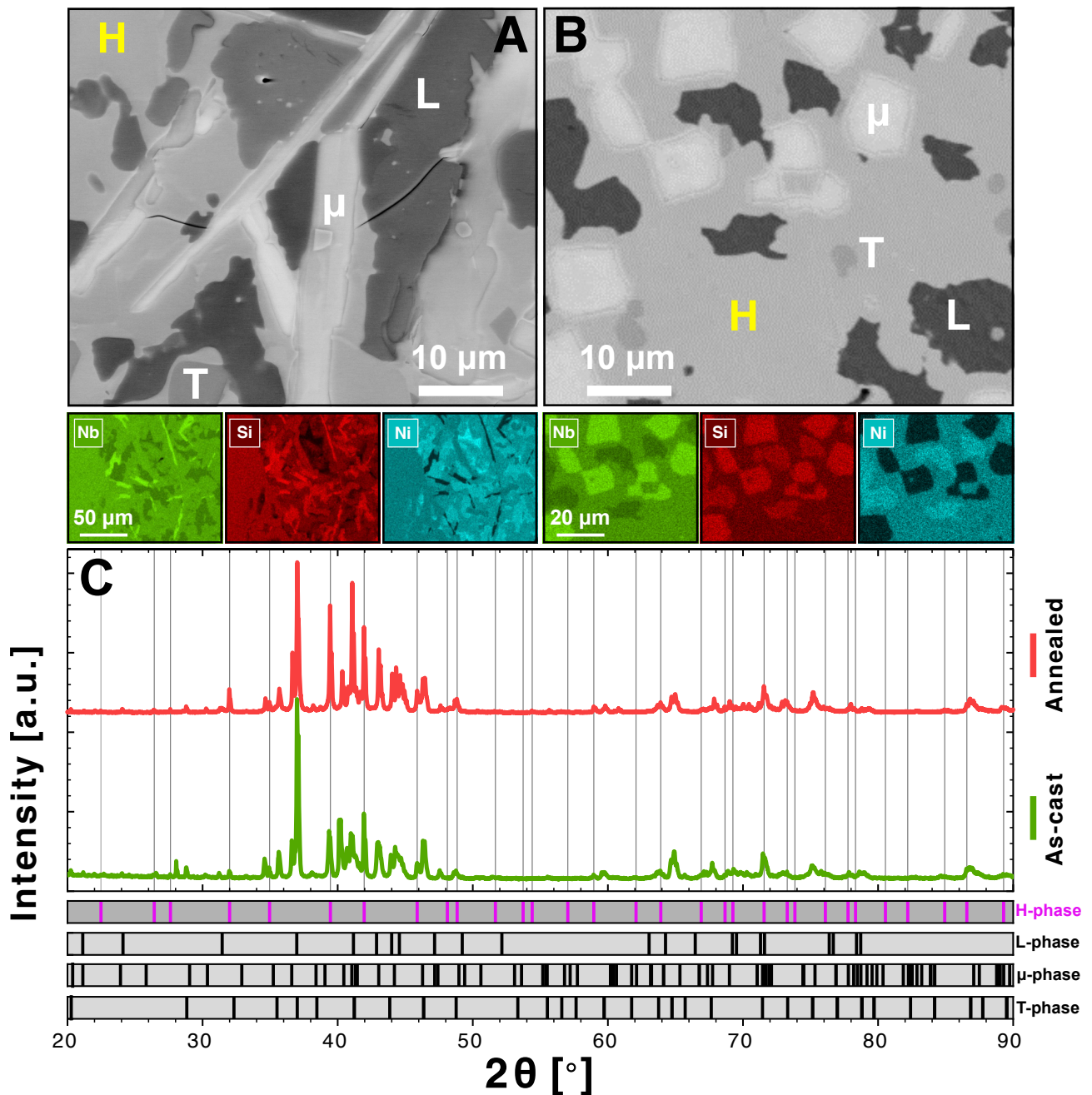


Figure 1: SEM/EDX and XRD characterization of the arc-melted Nb-Si-Ni intermetallic alloy in the as-cast state and after homogenization annealing at 1421 K for 336 h. BSE imaging and EDX elemental mapping of both as-cast (A) and annealed (B) samples show that the (thermodynamically metastable) arc-melted alloy comprises four distinct phases, *i.e.*, H-Nb₃SiNi₂, L-Ni₃SiNb₂, μ -Nb₇Ni₆ and T-Nb₄SiNi. (C) XRD patterns of the as-cast and annealed alloy samples confirm the presence of these four phases. The phase-of-interest, *i.e.*, the ternary H-phase Nb₃SiNi₂ IMC, is highlighted in both BSE micrographs and XRD spectra.

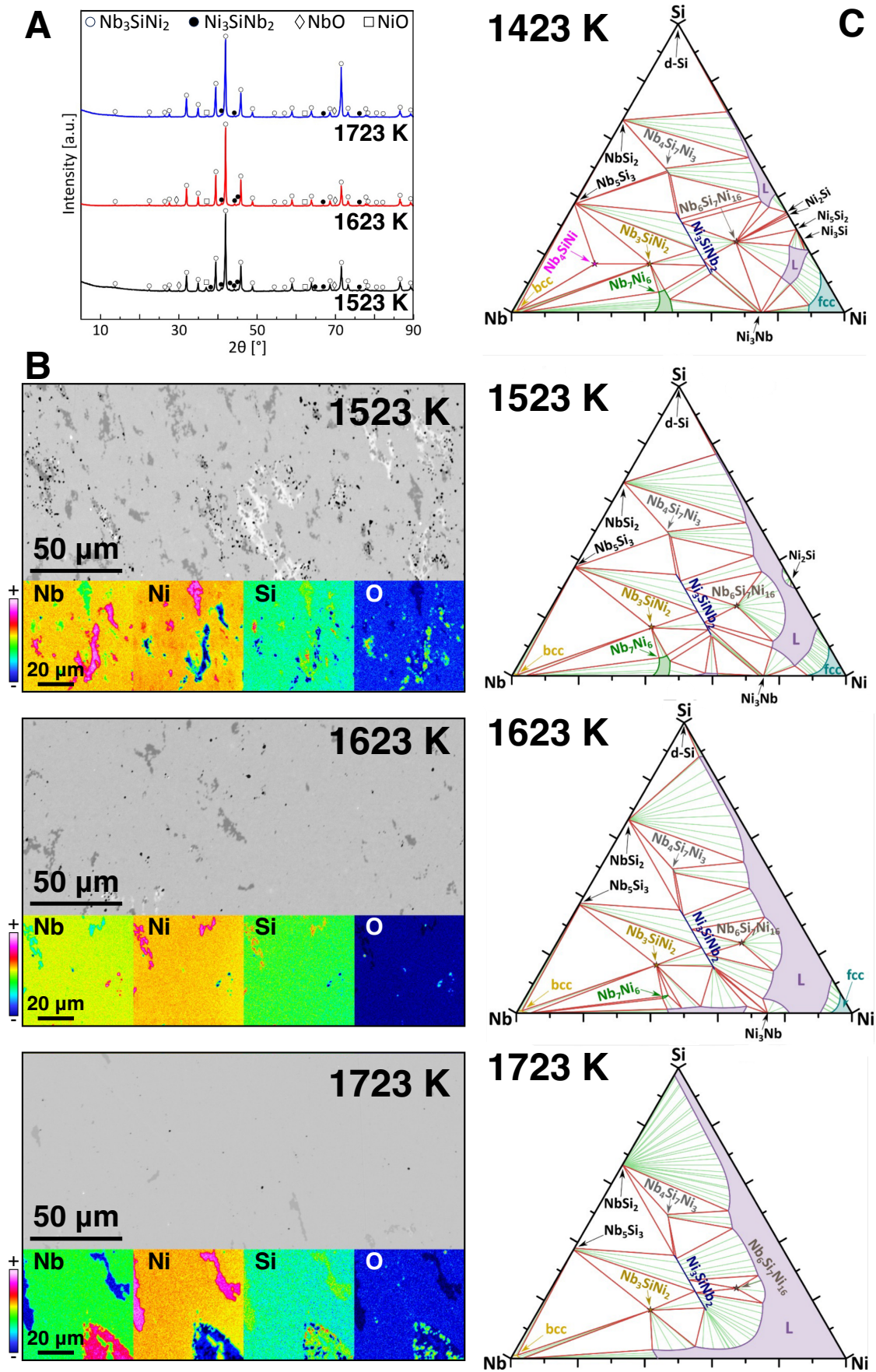


Figure 2: XRD (A) and SEM/WDXS (B) characterization of the RHP Nb-Si-Ni intermetallic alloy, showing that all alloy samples comprise mainly H- Nb_3SiNi_2 and L- Ni_3SiNb_2 , with small fractions of oxidic inclusions (NbO, NiO) presumably stemming from the limited powder particle oxidation. Microstructural homogeneity and phase purity (in terms of the desired Nb_3SiNi_2 ZIA phase) seem to increase with sintering temperature. (C) CALPHAD calculations of phase equilibria in the Nb-Si-Ni system on the 1423 K, 1523 K, 1623 K and 1723 K isotherms.

2.2. TEM/STEM characterization of the Nb_3SiNi_2

Even though arc melting produced a bulk sample with a low Nb_3SiNi_2 content, FIB was used to lift out thin foils from sufficiently large Nb_3SiNi_2 grains in the annealed sample (Fig. 3A) for characterization of the Nb_3SiNi_2 ZIA phase by means of (S)TEM/SAED. This characterization was decided before quasi-phase-pure bulk samples were produced via RHP, so as to gain a first in-depth understanding of the crystal structure of the Nb_3SiNi_2 ZIA phase. A bright-field STEM (BF-STEM) cross-sectional micrograph of such a Nb_3SiNi_2 grain is shown in Fig. 3A. The defects observed within the first 500 nm beneath the sample surface (protected by a combined Pt/C strip during FIB lift-out) are attributed to mechanical damage induced during grinding/polishing of the bulk annealed sample. The presence of sub-surface mechanical damage did not affect the chemistry of the analyzed grain, which was found by STEM/EDS to be compositionally homogeneous and close to the Nb_3SiNi_2 stoichiometry with limited deviations from the expected Ni (5 at.% excess) and Si (5 at.% deficiency) contents (Fig. 3B).

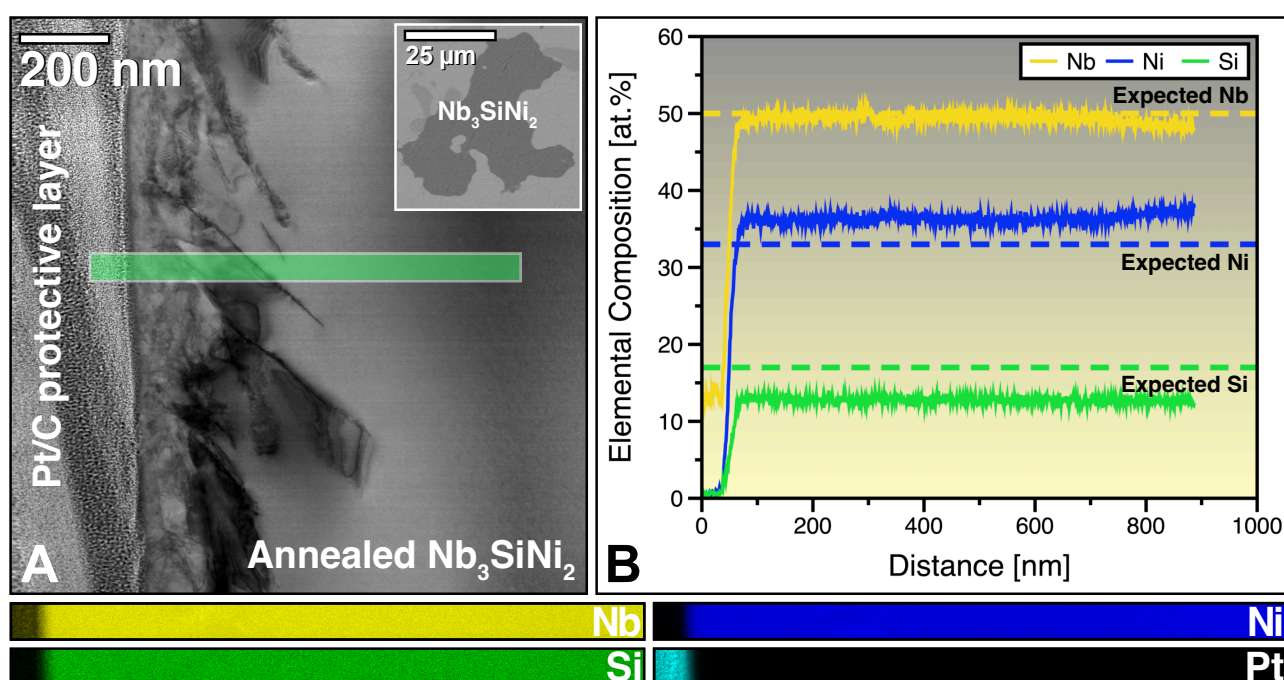


Figure 3: STEM/EDX analysis of a FIB foil lifted-out from a large Nb_3SiNi_2 IMC grain in the annealed arc-melted alloy. (A) BF-STEM micrograph of the Nb_3SiNi_2 IMC grain showing sub-surface mechanical damage caused by sample grinding/polishing. The inset is a BSE image of the Nb_3SiNi_2 grain selected for this FIB foil lift-out. (B) STEM/EDS analysis of the area inside the green rectangle of Fig. 3A shows the homogeneous distribution of Nb, Si and Ni (Nb/Si/Ni elemental maps, bottom), confirming that the average chemical composition of this grain within the analyzed area deviates slightly from the Nb_3SiNi_2 stoichiometry (Nb/Si/Ni profiles, top).

Given the rather satisfactory chemistry match with the targeted Nb_3SiNi_2 stoichiometry, further characterization of the same Nb_3SiNi_2 grain by STEM & SAED (selected area diffraction) was deemed necessary to elucidate the crystal structure. Figure 4A is an atomically resolved BF-STEM image of the Nb_3SiNi_2 ZIA phase, showing the nanolayered atomic arrangement in a “zigzag” pattern, which was observed in specific low-index crystallographic orientations. Figure 4B shows a SAEDP recorded after orienting the sample onto the low-index $[\bar{1}12]$ zone axis. Using published crystallographic data (CIF file code ICSD-2044323 [43]) and the SingleCrystal software package [52], a kinematic simulation of the SAEDP (Fig. 4D) was made and compared with the recorded SAEDP (Fig. 4B). Experimental and simulated SAEDPs were in excellent agreement, whilst all collected data suggested that the crystal structure

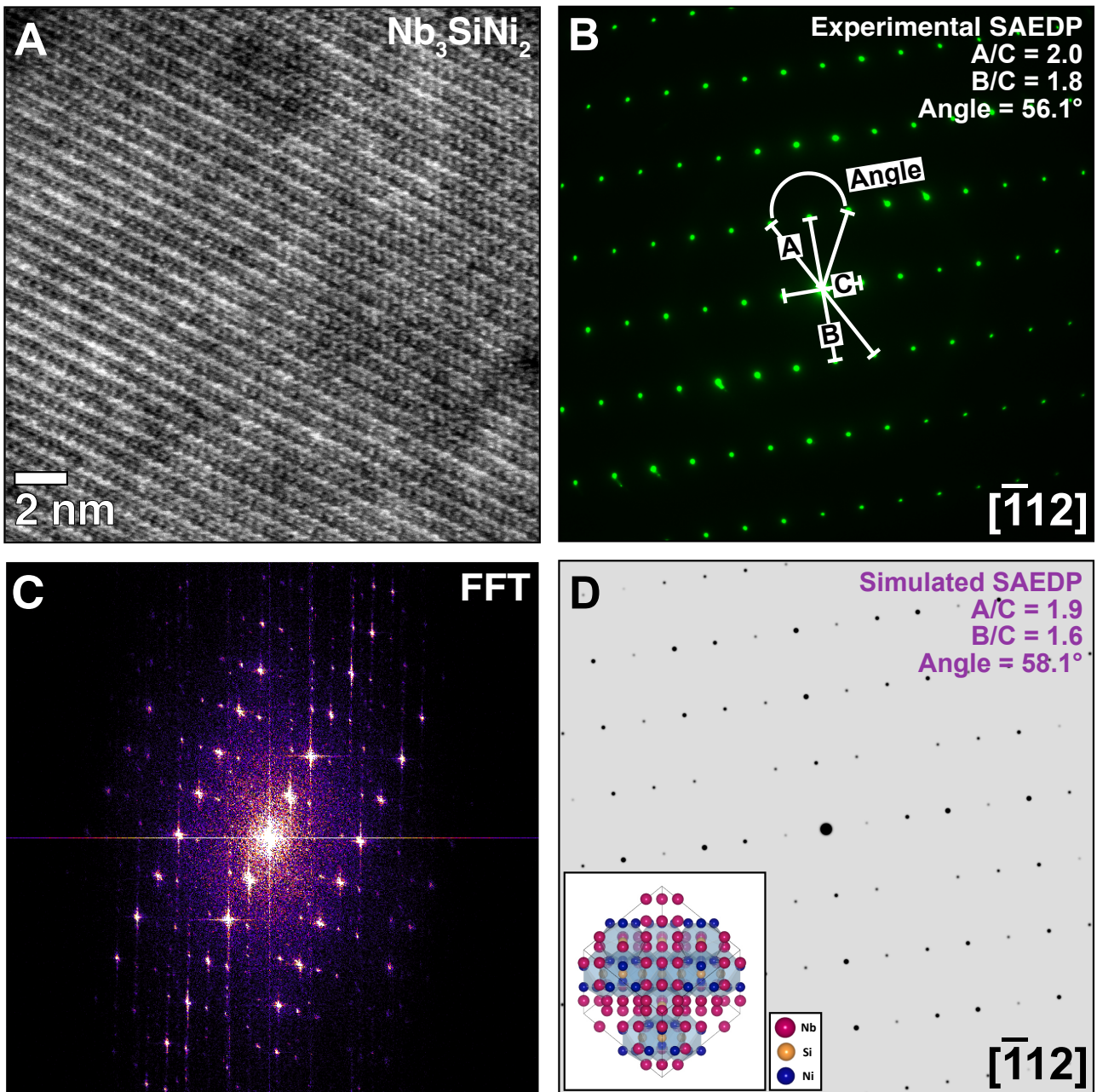


Figure 4: STEM/SAED characterization of the single Nb_3SiNi_2 IMC grain of Figure 3A. (A) High-resolution BF-STEM micrograph of the Nb_3SiNi_2 IMC grain viewed in the low-index $[\bar{1}12]$ zone axis. (B) Experimental SAEDP and (C) Fast Fourier Transform (FFT) pattern of the $[\bar{1}12]$ zone axis of the Nb_3SiNi_2 IMC. (D) Simulated SAEDP of the $[\bar{1}12]$ zone axis of the Nb_3SiNi_2 IMC; the inset presents the unit cell of the Nb_3SiNi_2 in the $[\bar{1}12]$ zone axis. The simulated SAEDP was produced using SingleCrystal [52] and experimental data that are available in the ICSD database [43]. The experimental and simulated SAEDPs of Figures 4B and 4D, respectively, confirm that the Nb_3SiNi_2 candidate ZIA phase has the diamond cubic crystal structure (fcc Bravais lattice; $Fd\bar{3}m$; space group 227).

of the experimentally synthesized Nb_3SiNi_2 is diamond cubic ($Fd\bar{3}m$, space group 227) [43]. This crystal structure characterizes not only the ternary H-phase (Nb_3SiNi_2) of the Nb–Si–Ni system [43, 45, 46], but also the ternary IMCs with identical stoichiometry in the Mn–Si–Ni (Mn_3SiNi_2) [43, 53, 54], V–Si–Ni (V_3SiNi_2) [43], Cr–Si–Ni (Cr_3SiNi_2) [43], Ta–Si–Ni (Ta_3SiNi_2) [43, 55], Nb–Si–Co (Nb_3SiCo_2) [56], Na–Au–In (Na_3AuIn_2) [12], Na–Ag–In (Na_3AgIn_2) [12], and Mg–Ga–Ni (Mg_3GaNi_2) [57] systems, apparently being the preferred crystal structure for the entire class of the (312) ZIA phases, just like the hexagonal close-packed (*hcp*; $P6_3/mmc$, space group 194) crystal structure encompasses all MAX phase compounds [6, 10]. Having said that, it is also worthwhile adding that few IMCs with the 312 stoichiometry and the *hcp* ($P6_3/mmc$, space group 194) crystal structure have been sporadically identified, possibly suggesting the existence of a not yet fully identified and/or explored overarching trend in the formation of nanolaminated solids, such as the known MAX phases and the herein proposed ZIA phases. Examples of ternary 312 IMCs with the *hcp* crystal structure have been previously reported in the Co–Si–Nb (Co_3SiNb_2) [56], Ni–Si–Nb (Nb_3SiNi_2) [43] and Cu–Si–Mg (Cu_3SiMg_2) [56] systems. In view of the scarcity of available data, it would be premature to speculate on the relation between the *fcc* ternary IMCs identified in this work as the ZIA phases and the largely unexplored *hcp* ternary IMCs, or to assume that the latter are also characterized by crystal structure nanolamination, even though such a hypothesis seems quite plausible.

2.3. Opportunities arising from the advent of the ZIA phases

In the search for new refractory materials with exceptional properties, both ZIA and MAX phases are nanolaminated crystalline solids that share the same historical roots, dating back to the advent of space exploration in the 1960s [7, 8, 43, 45, 46, 58]. Despite the fact that they have been both discovered in the same period of time, there is very little, if any, knowledge of the properties and possible applications of the ternary IMC ZIA phases and their (not yet synthesized) 2D derivatives, as opposed to the extensively studied MAX phase ternary carbides/nitrides, their higher order solid solutions and 2D derivatives known as MXenes. Therefore, this section will attempt to describe the basic differences and similarities of the rather mature MAX phases vs. the emerging ZIA phases, discussing potential applications of the latter based on the experience gained through the MAX-phase research over the past 30 years.

Using data compiled by the Materials Genome Project [59], the first candidate ZIA phase, *i.e.*, the Nb_3SiNi_2 IMC, is herein discussed with respect to the extensively studied Ti_3SiC_2 MAX phase. First, they are both ternary compounds that belong to different elemental systems, *i.e.*, Nb_3SiNi_2 forms in the Nb–Si–Ni system, while Ti_3SiC_2 in the Ti–Si–C system. Even though both compounds obey the 312 MAX phase stoichiometric rule, *i.e.*, $\text{M}_{n+1}\text{AX}_n$ with $n = 2$, Nb_3SiNi_2 is clearly an IMC, while Ti_3SiC_2 is classified as a ceramic. Moreover, there is a remarkable difference in crystal structure complexity, with the unit cell of the Nb_3SiNi_2 ZIA phase (Fig. 5A) being significantly larger than the unit cell of the Ti_3SiC_2 MAX phase (Fig. 5B). More specifically, the Ti_3SiC_2 unit cell is made of 6 atoms, while the Nb_3SiNi_2 one is made of 96 atoms, resulting in unit cell volumes that differ in size by one order of magnitude (Table S1 in the Supplementary Information). Both ternary compounds are characterized by centrosymmetric close-packed Bravais lattices, *i.e.*, the Ti_3SiC_2 MAX phase is *hcp* ($P6_3/mmc$, space group 194) whilst the Nb_3SiNi_2 ZIA phase is *fcc* (face-centered cubic; $Fd\bar{3}m$, space group 227); apparently, such close-packed atomic configurations seem to favor crystal structure nanolamination.

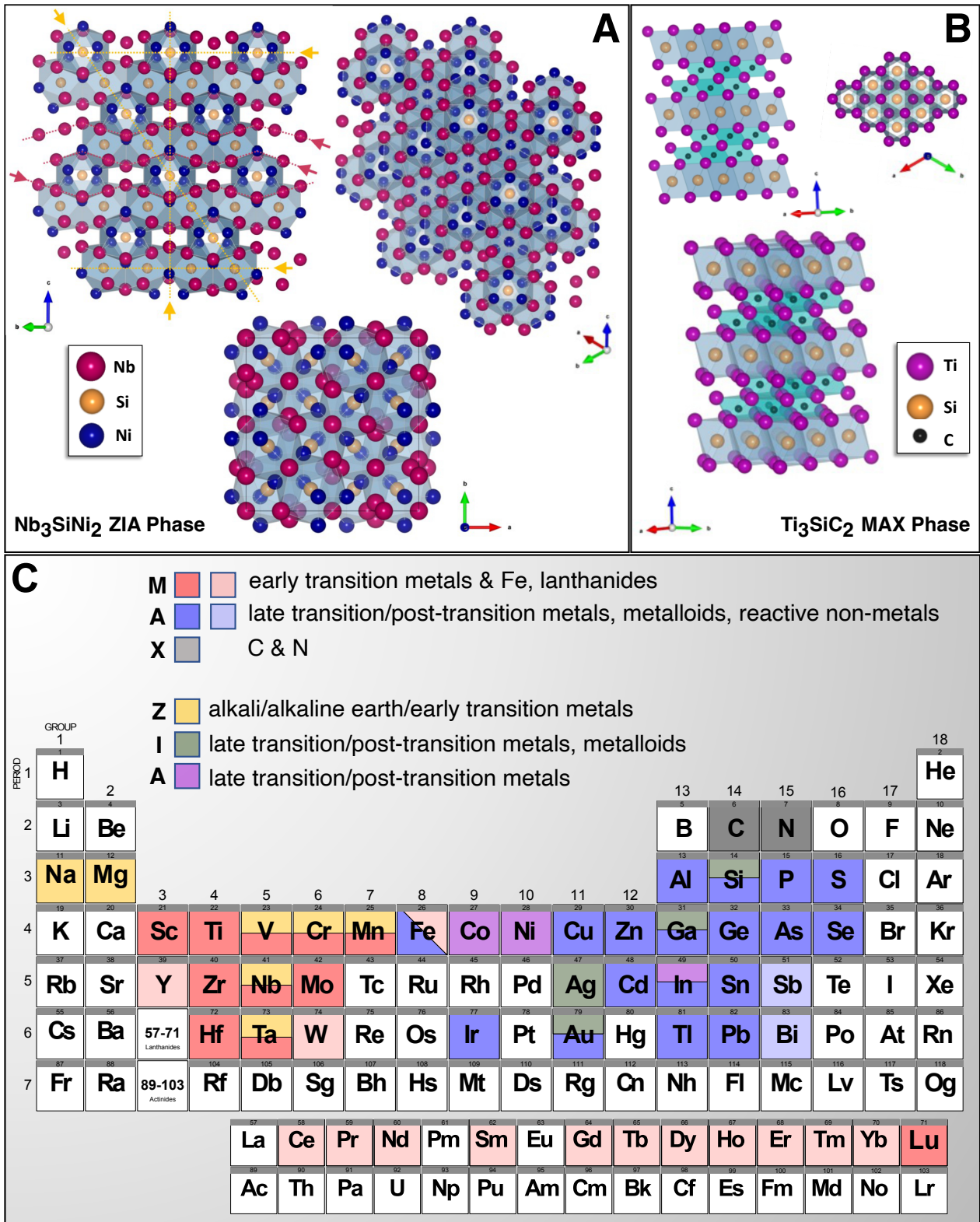


Figure 5: Comparison of the unit cells of (A) the herein synthesized and characterized *fcc* Nb₃SiNi₂ ZIA phase with (B) the well-known *hcp* Ti₃SiC₂ MAX phase [5, 8]. Fig. 5A (bottom) shows 1 unit cell (96 atoms/unit cell) of the Nb₃SiNi₂ ZIA phase, as well as the [110] (upper left) and [111] (upper right) zone axes using 4 unit cells. Red arrows pinpoint atomic zigzagging in the [110] zone axis, yellow arrows indicate crystal structure nanolamination. Fig. 5B (bottom) shows 8 unit cells of the Ti₃SiC₂ MAX phase (6 atoms/unit cell), as well as the [11̄20] (upper left) and [0001] (upper right) zone axes. (C) The ZIA phases extend the concept of crystal structure nanolamination beyond the early transition metal carbides/nitrides known as the MAX phases. Together, the two classes of nanolaminated solids span almost the whole period table, comprising jointly elements from groups 1-16. The M-elements of the MAX phases are shown using 2 shades of red: the darker indicates full occupation of the M-site, the lighter indicates partial occupation (solid solutions). The same holds for the 2 shades of blue dedicated to the A-elements of the MAX phases. Note: the periodic table in Fig. 5C is a modified version of the original American Chemical Society's periodic table.

A groundbreaking impact of the herein proposed ZIA phases is that they actually extend the concept of crystal structure nanolamination much beyond the early transition metal carbides/nitrides known as the MAX phases. As may be seen in the color-coded periodic table of elements of Fig. 5C, the M-elements used to form ternary MAX phases are early transition metals (groups 3-7), the A-elements belong mainly to groups 13-15 (post-transition metals & metalloids) with limited expansion to groups 8-12 (late transition metals) and group 16 (reactive non-metals), while the X-element is either C or N (reactive non-metals in groups 14 and 15, respectively). On the other hand, the ZIA IMCs that have been hitherto identified utilize Z-elements from groups 1 (alkali metals) and 2 (alkaline earth metals) and groups 5-7 (early transition metals), I-elements from group 11 (late transition metals) and groups 13 and 14 (post-transition metals & metalloids), while the A-elements belong either to groups 9 and 10 (late transition metals) or group 13 (the post-transition metal indium, In). In short, the synthesis of nanolaminated crystalline solids (MAX and ZIA phases) requires different combinations of constituent elements from groups 1-16 in the periodic table. This heralds the potential fabrication of ternary compounds and higher-order solid solutions with unique properties and very broad applicability, not only in the form of the 3D ZIA and MAX phases, but also in the form of their 2D derivatives, which have so far only been explored for the MAX phases in the form of the rapidly developing MXenes. Especially the discovery of ZIA phases comprising elements that have hitherto not been introduced in the MAX phases (e.g., alkali and alkaline earth metals, several late transition metals) paves the way for the fabrication of new nanolaminated crystalline solids with certain properties (e.g., ferromagnetic properties, enhanced/tailorable ductility, superconductivity, etc.) that are typically not associated with the MAX phases. This hypothesis finds support in the work of Kolenda *et al.* [54], who reported on the magnetic properties of the Mn_3SiNi_2 candidate ZIA phase. The new range of properties achieved by the ZIA phases is also expected to be reflected in their 2D derivatives (assuming these can first be produced experimentally), probably giving rise to the next generation of 2D materials for use in flexible and portable microelectronics, batteries, sensors, etc.

It is worthwhile noting that in all hitherto reported *fcc* ternary IMCs now considered as candidate ZIA phases, the electronegativity, χ , of the Z-element is invariably smaller than the electronegativities of both I- and A-elements (Table S2 in the Supplementary Information). Moreover, the atomic radius of the Z-element is larger than the atomic radii of both I- and A-elements with the exception of Cr_3SiNi_2 , where the atomic radius (125 pm) of the Z-element, Cr, is equal to that of the A-element, Ni (Table S2 in the Supplementary Information). Interestingly, the structurally unexplored 312 *hcp* ternary IMCs Co_3SiNb_2 and Ni_3SiNb_2 could be considered as 'compositionally inverted' Nb_3SiCo_2 and Nb_3SiNi_2 ZIA phases, respectively, produced by interchanging the Z- and A-elements while still respecting the strict stoichiometric rule of the 312 MAX phases. For these two *hcp* IMCs as well as for the Cu_3SiMg_2 one, the electronegativity of the third element (Nb or Mg) is smaller than the electronegativities of the first two elements (Co, Ni or Cu). Also, the atomic radius of the third element (Nb or Mg) is larger than the atomic radii of the first two elements (Co, Ni or Cu). Based on these structural considerations and the fact that the *hcp* ternary IMCs Co_3SiNb_2 , Ni_3SiNb_2 and Cu_3SiMg_2 are characterized by the same hexagonal close-packed lattice ($P6_3/mmc$, space group 194) as the MAX phases, one could indeed expect crystal structure nanolamination in these ternary IMCs as well. This hypothesis, however, merits further dedicated investigation.

A unique feature of the ZIA phases is that the I- and A-elements could be chosen from the same group in the periodic table. For example, both the A-element (In) in Na_3AuIn_2 , and Na_3AgIn_2 as well as the I-element (Ga) in Mg_3GaNi_2 belong to group 13. This freedom in the choice of the elements making up the ZIA phases does not characterize the MAX phases, where only two X-elements are allowed (*i.e.*, C or N), and these are not known to be replaced by any of the candidate M- and A-elements. The only known exception of an element that has been rather flexible in occupying the M- or A-site of specific MAX phase compounds is the late transition metal iron (Fe), which belongs to group 8 of the periodic table. More specifically, Fe has been fairly recently reported to form the $(\text{Ti}_{1-x}, \text{Fe}_x)_3\text{AlC}_2$ solid solutions on the M-site [60], or to occupy fully the A-site of the ternary MAX phases Ta_2FeC , Ti_2FeN and Nb_2FeC [61]. With respect to the ZIA phases, the allowable combinations of elemental constituents could probably be associated with differences in the electronegativity and atomic radius values of the Z-, I- and A-elements; however, before definitive rules governing the ZIA phase formation can be proposed, further systematic research is needed to better map – in terms of attainable chemical compositions – the ZIA phases ‘landscape’.

Even though the main objective of this work was to introduce the class of nanolaminated ZIA phases via the experimental synthesis and characterization of its Nb_3SiNi_2 first candidate member as well as to demonstrate the feasibility of producing phase-pure materials based on the Nb_3SiNi_2 ternary IMC, an overarching stoichiometric rule governing both the MAX and the ZIA phases was discovered and is proposed here. As pointed out by Goossens et al. in a rather recent review [10], the nanolaminated MAX phases are mainly encountered either as the three well-known $\text{M}_{n+1}\text{AX}_n$ phase orders 211, 312 and 413, or as the following exceptional structures: (i) the $\text{M}_{n+1}\text{AX}_n$ -like structures with $n > 3$, such as Ta_6AlC_5 and Ti_7SnC_6 , and (ii) the “hybrid” orders $\text{M}_5\text{A}_2\text{C}_3$ and $\text{M}_7\text{A}_2\text{C}_5$, such as $\text{Ti}_5\text{A}_2\text{C}_3$ with A = Si, Ge and Al. To date, the “hybrid” orders $\text{M}_5\text{A}_2\text{C}_3$ and $\text{M}_7\text{A}_2\text{C}_5$ have been considered as combinations of a 312 atomic stacking with a 211 and a 413 order, respectively, as they did not obey the generic $\text{M}_{n+1}\text{AX}_n$ phase stoichiometry. However, the careful consideration of both the 312 ZIA phases and all the MAX phase variants, including the “hybrid” orders and the only identified member of the 514 order, *i.e.*, *i.e.*, the Mo_4VAIC_4 compound [62], revealed that both classes of nanolaminated crystalline solids with *fcc* and *hcp* close-packed lattices can be described by the general stoichiometric rule $\text{P}_{x+y}\text{A}_x\text{N}_y$ (PAN), where $x = 1$ or 2 , and $y = 1, 2, 3, 4, 5$, or 6 , according to all the ‘PAN phases’ that were experimentally synthesized to date. The herein proposed global stoichiometric rule governs the constitution of all nanolaminated crystalline solids with atomically close-packed lattices, such as the *fcc* ZIA phases, the *hcp* MAX phases and the ternary *hcp* IMCs, such as Co_3SiNb_2 , Ni_3SiNb_2 and Cu_3SiMg_2 , even though crystal structural nanolamination has still not been confirmed for the latter. Moreover, this global stoichiometric rule reconciles the “hybrid” orders $\text{M}_5\text{A}_2\text{C}_3$ and $\text{M}_7\text{A}_2\text{C}_5$ with the common MAX ($\text{M}_{n+1}\text{AX}_n$) phase orders 211, 312 and 413, providing an affirmative answer to the question whether it was conceptually correct to include all identified MAX phase variants in the same class of materials.

A major challenge addressed in this work was to demonstrate that the synthesis of phase-pure bulk ZIA phase-based materials is feasible. Producing phase-pure bulk materials is a prerequisite for the systematic investigation of material properties (*e.g.*, elastoplastic and fracture behavior; oxidation and corrosion resistance; electrical and magnetic properties; radiation tolerance; etc.) or the possible appli-

cations of the ZIA phases and their 2D derivatives, provided that these can be extracted. Even though the production of phase-pure Ni_3SiNb_2 via arc melting proved extremely challenging, presumably due to the volatilization of Ni and/or its compounds above a certain temperature, the synthesis of quasi-phase-pure bulk Ni_3SiNb_2 via RHP was successful. Similar challenges in producing phase-pure bulk materials have been previously reported in association with the synthesis of specific MAX phases, such as the Zr- and Hf-based MAX phases [19, 20, 37, 39, 63, 64]; typically, overcoming these challenges involved the synthesis of complex double solid solutions based on steric stability criteria [39, 65], or the use of early transition metal hydride raw powders rather than elemental ones [51]. Apart from RHP, several other processing methods will be explored to synthesize phase-pure ZIA phases in various forms (bulk, coatings) so as to make progress with structural characterization, property determination and possible applications. Physical vapor deposition (PVD) coating techniques, such as magnetron sputtering, are expected to be able to deposit coatings of very precise compositions, such as the herein studied Ni_3SiNb_2 ZIA phase onto substrates of choice, suppressing the formation of competing phases and producing phase-pure coatings with strong textures that might be desired by certain high-tech applications.

3. Conclusions

Nanostructured materials have revolutionized modern materials science, even though their potential is far from being fully exploited for the benefit of the Society. Nanolaminated ceramics, such as the MAX phases and their 2D derivatives known as MXenes, already changed the way we perceive materials design and functionalization on the nanoscale, thereby producing innovative materials that are characterized by a wide variety of unique properties, precisely tailored to the requirements of the targeted applications. Identifying market niches that could use nanostructured materials, including applications in extreme service environments (*e.g.*, high temperatures and pressures, corrosive media, irradiation, etc.), is an important driver towards the commercial deployment of innovative materials with sophisticated nanodesigns and carefully engineered functionalities. In this work, we propose a novel class of nanolaminated crystalline solids, the ‘zigzag intermetallic’ phases or, simply, the ZIA phases. The herein introduced ZIA phases are characterized by an *fcc* ($Fd\bar{3}m$, space group 227) close-packed lattice of appreciable structural complexity, while obeying the stoichiometric rule of the 312 MAX phases, *i.e.*, $\text{M}_{n+1}\text{AX}_n$ with $n = 2$. The ZIA phases and all known MAX phase orders, including the “hybrid” $\text{M}_5\text{A}_2\text{C}_3$ and $\text{M}_7\text{A}_2\text{C}_5$ ones mentioned above, appear to respect the herein proposed global stoichiometric rule $\text{P}_{x+y}\text{A}_x\text{N}_y$, where x and y are integers in the 1-6 range.

The first candidate ZIA phase, *i.e.*, the Nb_3SiNi_2 IMC, is identified as the H-phase of the Nb–Si–Ni system and has been found in bulk samples fabricated by both arc melting (low Nb_3SiNi_2 content) and RHP (quasi-phase-pure Nb_3SiNi_2). The STEM/SAED characterization of Nb_3SiNi_2 confirmed the expected diamond cubic crystal structure, revealing a remarkable structural complexity, as reflected in an exceptionally large unit cell made of 96 atoms with nanolayered arrangement. Considering that, apart from the Nb_3SiNi_2 IMC, other ternary 312 IMCs (*i.e.*, Mn_3SiNi_2 , V_3SiNi_2 , Cr_3SiNi_2 , Ta_3SiNi_2 , Nb_3SiCo_2 , Na_3AuIn_2 , Na_3AgIn_2 , and Mg_3GaNi_2) with the same diamond cubic *fcc* lattice have already been experimentally synthesized, it is reasonable to assume that these IMCs constitute an entire class of nanolaminated crystalline solids, herein designated as the ZIA phases. Confirming the nanolaminated nature of

the other ternary 312 IMCs is the aim of ongoing investigations.

The ZIA phases extend the concept of crystal structure nanolamination beyond the early transition metal carbides/nitrides known as the MAX phases. Despite sharing similarities and the same historical roots with the MAX phases, ZIA phases such as the Nb_3SiNi_2 IMC are characterized by appreciably more complex crystal structures and, by extension, configurational entropies than ternary MAX phases such as the Ti_3SiC_2 ceramic. Therefore, the nanolaminated ZIA phases are conceptually positioned, in terms of characteristics and potential applications, between the nanolaminated MAX phases (with unique hybrid metallic/ceramic properties, and proven capability of producing 2D derivatives, known as MXenes, with tailored functionalities) and other dense and complex multicomponent alloys, such as high-entropy alloys (HEAs) characterized by large chemical complexity and remarkable radiation tolerance. This work succeeded in synthesizing phase-pure bulk Nb_3SiNi_2 via reactive hot pressing (RHP), which is considered an important achievement as the production of phase-pure ZIA phase-based materials is not only a prerequisite for the (mechanical, electrical, magnetic, etc.) property determination of these largely unknown compounds, but also to explore the possibility of producing and characterizing their (potential) 2D derivatives, as well as assessing ways to tailor their properties (e.g., ductility) in an application-driven manner. It is likely that the new class of ZIA phases will create a new ecosystem of nanolaminated/nanostructured (3D/2D) materials with amazing new properties and fascinating applications in diverse technological areas. The first step towards the exploration of this hitherto unexplored ecosystem is the successful synthesis of many materials with high phase purity, starting from the already identified candidate ZIA phases (e.g., Nb_3SiNi_2 , Mn_3SiNi_2 , V_3SiNi_2 , Cr_3SiNi_2 , Na_3AuIn_2 , Mg_3GaNi_2 , etc.) and proceeding with theoretically predicted (e.g., by means of thermodynamic modeling, density functional theory, etc.) but not yet experimentally made IMCs. The second step in this exploratory work should include attempts to produce 2D derivatives of the ZIA phases, as well as ternary *hcp* IMCs (e.g., Co_3SiNb_2 , Ni_3SiNb_2 , Cu_3SiMg_2 , etc.), in order to find out whether they are also characterized by crystal structure nanolamination, as expected, or not.

4. Experimental Section

4.1. Synthesis via Arc Melting

Conventional vacuum arc melting of high-purity (>99.99%) Nb, Ni and Si elemental raw powders was initially employed to synthesize the 'Nb–Si–Ni intermetallic alloy' with the targeted H-phase Nb_3SiNi_2 stoichiometry, *i.e.*, 50.0Nb-16.7Si-33.3Ni¹, in at.%. A disc (200 g) of low phase purity was produced via arc melting, despite the fact that the ratio of elemental powders in the powder feedstock had been adjusted to the Nb_3SiNi_2 stoichiometry. Additional information on the arc melting synthesis of alloys in the Nb–Si–Ni system may be found elsewhere [44–46].

The thermal and microstructural stability of the as-cast Nb–Si–Ni intermetallic alloy was assessed via an isothermal annealing treatment at 1421 K for 2 weeks (336 h) in a vacuum furnace (ThermoLyne furnace, model 46100). The as-cast alloy samples were pre-encapsulated in a quartz (SiO_2) tube, which was pressurized with argon (Ar) gas to 1 atm; both heating and cooling rates were fixed at about 14.2 K/min.

¹The term "Nb–Si–Ni intermetallic alloy" is used for this alloy composition throughout the manuscript.

4.2. Synthesis via Reactive Hot Pressing

The inability to produce a phase-pure Nb–Si–Ni intermetallic alloy by means of arc melting redirected the synthesis efforts in this work towards a powder metallurgical processing route. Quasi phase-pure discs of the Nb–Si–Ni intermetallic alloy were successfully produced via reactive hot pressing (RHP), using hydride and elemental starting powders, *i.e.*, NbH_{0.89} (<40 μm, CBMM, Brazil), Ni (Vale, T123™, 3-7 μm, UK) and Si (A10, 2.1 μm, HC Starck, Germany). To optimize the mixing of the starting powders and improve powder particle contact, the as-received NbH_{0.89} powder was first refined by low-energy ball milling in isopropanol for 24 h (Turbula®T2), using WC-6 wt.% Co (WC-6Co) milling balls (diameters of 5 and 10 mm). The refined NbH_{0.89} powder was dried in a rotating evaporator (Heidolph 4010) and then mixed with the Ni and Si elemental powders in isopropanol for another 24 h, using WC-6Co balls. The ratio of the NbH_{0.89}, Ni and Si powders in the powder feedstock was adjusted to the targeted 3Nb:1Si:2Ni. After mixing, the powder suspension was dried in a rotating evaporator.

The powder feedstock was cold-pressed into 'green' pellets (30 mm in diameter, 4-5 mm thickness) under a load of 30 MPa in a graphite die. Exploratory RHP runs were carried out in a hot press (W100/150-2200-50 LAX, FCT Systeme, Frankenblick, Germany). The powder compacts were heated in vacuum (0.4 mbar) at 10 K/min to different sintering temperatures (*i.e.*, 1523, 1623 and 1723 K), where consolidation occurred under an uniaxial pressure of 30 MPa for a dwell period of 60 min. The sintered discs (30 mm in diameter) were allowed to cool naturally by switching off the power supply of the hot-press.

4.3. Materials Characterization

Metallographic cross-sections were prepared from all Nb–Si–Ni intermetallic alloy samples produced via arc melting and RHP; all cross-sections were polished to a mirror surface finish with a colloidal silica (OPS) suspension in the final step. The microstructure of as-cast and isothermally annealed samples produced via arc melting was studied by means of a Thermo Fisher Apreo SEM (scanning electron microscope) equipped with an EDX (energy-dispersive X-ray spectroscopy) detector (EDAX Octane Elite Super). Elemental mapping in the RHP samples was done by means of an electron probe microanalyzer (EPMA; JXA-8530F, JEOL Ltd, Japan) equipped with a WDXS (wavelength-dispersive X-ray spectroscopy) detector (1-5 eV, 8 eV at Fe-K_α, full scanner type spectrometer). EDX elemental analysis (1 SDD/UTW, 129 eV at Mn-K_α) of the identified phases was performed on the same device at fixed conditions (15 kV accelerating voltage, 100 nA beam current).

X-ray diffraction (XRD) was employed to identify the phases present in all Nb–Si–Ni intermetallic alloy samples at room temperature. The as-cast and annealed samples produced via arc melting were analyzed on a Bruker AXS D8 Advance X-ray diffractometer, using Cu-K_α radiation (40 kV, 40 mA) in a Bragg-Brentano geometry; the XRD spectra were recorded at steps of 0.02° in the 20-90° 2θ range. The RHP samples were analyzed on a Rigaku SmartLab SE XRD system with 1D/teX Ultra 250 HE detector, using Cu-K_α radiation (40 kV, 40 mA) in a Bragg-Brentano geometry; the XRD spectra were recorded at steps of 0.05° in the 5-90° 2θ range, at a scan speed of 0.1° per min.

An FEI Helios 600 dual-beam FIB/SEM was used to lift out TEM (transmission electron microscopy) thin foils from sufficiently large Nb₃SiNi₂ grains in the arc-melted alloy samples, utilizing the classic lift-out method [66]. Combined Pt/C protective capping layers were deposited on the sites of interest to

protect the foils from ion beam damage during lift-out. The FIB (focused ion beam) foils were ion-milled to electron transparency at 30 keV, with final thinning/ion beam damage removal at 2 keV.

TEM analysis of the FIB foils lifted out from the arc-melted alloy samples was performed by means of a FEI Tecnai TF30 and a FEI Titan 80/300, both operated at 300 kV. The latter was equipped with an EDAX Octane Elite T EDX detector, and all EDX quantification work was conducted based on the Cliff-Lorimer method [67, 68]. Selected area electron diffraction patterns (SAEDPs) of the Nb₃SiNi₂ IMC ZIA phase were indexed using data from the Inorganic Crystal Structure Database (ICSD) [43]. The CrystalMaker, SingleCrystal and CrystalDiffraction software packages were used to simulate electron diffraction patterns and aid the indexing of experimentally acquired SAEDPs [52].

4.4. Thermodynamic & Crystal Structure Simulations

Thermodynamic simulations were performed to predict the equilibrium phases at the sintering temperatures of the RHP alloys (*i.e.*, 1523 K, 1623 K, and 1723 K), as well as at 1423 K (*i.e.*, close to the homogenization annealing temperature, 1421 K, of the arc-melted alloy). These simulations were performed with version V2020a of the Thermo-Calc software (Thermo-Calc Software Inc., Solna, Sweden) [69], based on the database published by dos Santos *et al.* [44]. The unit cells of the *fcc* Nb₃SiNi₂ ZIA phase and the *hcp* Ti₃SiC₂ MAX phase were drawn using version 3.5.8 of the VESTA software [70], utilizing the Wyckoff parameters provided in Table S1 (Supplementary Information) for precise crystal structure representation. These two phases were compared in terms of relative structural complexity and unit cell sizes, whilst certain zone axes of the herein addressed Nb₃SiNi₂ ZIA phase were selected to depict 'zigzag' atomic arrangement and crystal structure nanolamination.

Acknowledgments

The Los Alamos National Laboratory (LANL), an affirmative action equal opportunity employer, is managed by Triad National Security, LLC, for the U.S. Department of Energy's National Nuclear Security Administration, under contract number 89233218CNA000001. LANL provided research support to MAT via the Laboratory Directed Research and Development (LDRD) program, under project number 20200689PRD2. OEA acknowledges funding from his Early Career Program supported by LANL's LDRD, under contract number 20210626ECR. CGS thanks the financial support provided by the Conselho Nacional de Desenvolvimento Científico e Tecnológico (CNPq, Brasília-DF, Project 307627/2021-7). MAT would like to thank Dr. Kurt E. Sickafus, LANL, for valuable discussions on the crystallography of complex solid-state phases. KL and JV acknowledge funding from the Euratom research and training program 2014-2018 under Grant Agreement No. 740415 (H2020 IL TROVATORE). NG acknowledges the Fund for Scientific Research Flanders (FWO-Vlaanderen) for funding his PhD Fundamental Research Fellowship No 1118120N.

Author Contributions

The initially devised experimental plan that employed arc melting to explore the precursor idea of the ZIA phases was formulated by MAT as a project for a Director's fellowship at LANL. MAT and KL share the conceptualization of the major scientific ideas associated with the class of nanolaminated ternary IMCs herein identified as the ZIA phases as well as their correlation with the class of nanolaminated early

transition metal carbides/nitrides known as the MAX phases. SH, NG, and JV succeeded in producing quasi-phase-pure Nb₃SiNi₂ materials by means of RHP. All other authors have smaller contributions with experiments, data analysis, research supervision, and funding. All authors have read and approved the manuscript. MAT started the first draft and KL extensively revised it, contributing with key ideas and RHP data, the latter in collaboration with KU Leuven.

References

References

- [1] R. W. Cahn, Nanostructured materials, *Nature* 348 (6300) (1990) 389–390.
- [2] H. Gleiter, Nanostructured materials, *Advanced Materials* 4 (7-8) (1992) 474–481.
- [3] P. Moriarty, Nanostructured materials, *Reports on Progress in Physics* 64 (3) (2001) 297.
- [4] F. J. Martin-Martinez, K. Jin, D. López Barreiro, M. J. Buehler, The rise of hierarchical nanostructured materials from renewable sources: learning from nature, *ACS Nano* 12 (8) (2018) 7425–7433.
- [5] M. W. Barsoum, T. El-Raghy, Synthesis and characterization of a remarkable ceramic: Ti_3SiC_2 , *Journal of the American Ceramic Society* 79 (7) (1996) 1953–1956.
- [6] M. W. Barsoum, T. El-Raghy, The MAX phases: Unique new carbide and nitride materials: Ternary ceramics turn out to be surprisingly soft and machinable, yet also heat-tolerant, strong and lightweight, *American Scientist* 89 (4) (2001) 334–343.
- [7] W. Jeitschko, H. Nowotny, F. Benesovsky, Kohlenstoffhaltige ternäre Verbindungen (H-phase), *Monatshefte für Chemie und verwandte Teile anderer Wissenschaften* 94 (4) (1963) 672–676.
- [8] W. Jeitschko, H. Nowotny, Die kristallstruktur von Ti_3SiC_2 —ein neuer komplexcarbidgebilde Typ, *Monatshefte für Chemie—Chemical Monthly* 98 (2) (1967) 329–337.
- [9] M. Sokol, V. Natu, S. Kota, M. W. Barsoum, On the chemical diversity of the MAX phases, *Trends in Chemistry* 1 (2) (2019) 210–223.
- [10] N. Goossens, B. Tunca, T. Lapauw, K. Lambrinou, J. Vleugels, MAX Phases, Structure, Processing, and Properties, in: M. Pomeroy (Ed.), *Encyclopedia of Materials: Technical Ceramics and Glasses*, Elsevier, Oxford, 2021, pp. 182–199.
- [11] M. Dahlqvist, A. Petruhins, J. Lu, L. Hultman, J. Rosén, Origin of chemically ordered atomic laminates (i-MAX): expanding the elemental space by a theoretical/experimental approach, *ACS Nano* 12 (8) (2018) 7761–7770.
- [12] B. Li, J. D. Corbett, Participation of sodium in the bonding of anionic networks: Synthesis, structure, and bonding of Na_3MIn_2 (M = Au, Ag), *Inorganic Chemistry* 44 (19) (2005) 6515–6517.
- [13] M. Naguib, M. Kurtoglu, V. Presser, J. Lu, J. Niu, M. Heon, L. Hultman, Y. Gogotsi, M. W. Barsoum, Two-dimensional nanocrystals produced by exfoliation of Ti_3AlC_2 , *Advanced Materials* 23 (37) (2011) 4248–4253.
- [14] M. Naguib, O. Mashtalir, J. Carle, V. Presser, J. Lu, L. Hultman, Y. Gogotsi, M. W. Barsoum, Two-dimensional transition metal carbides, *ACS Nano* 6 (2) (2012) 1322–1331.
- [15] Y. Gogotsi, B. Anasori, The rise of MXenes, *ACS Nano* 13 (8) (2019) 8491–8494.
- [16] Z. Wu, T. Shang, Y. Deng, Y. Tao, Q.-H. Yang, The assembly of MXenes from 2D to 3D, *Advanced Science* 7 (7) (2020) 1903077.
- [17] Y. Long, Y. Tao, T. Shang, H. Yang, Z. Sun, W. Chen, Q.-H. Yang, Roles of metal ions in MXene synthesis, processing and applications: a perspective, *Advanced Science* 9 (12) (2022) 2200296.
- [18] M. Ghebouli, B. Ghebouli, M. Fatmi, A. Bouhemadou, Theoretical prediction of the structural, elastic, electronic and thermal properties of the MAX phases X_2SiC (X = Ti and Cr), *Intermetallics* 19 (12) (2011) 1936–1942.
- [19] T. Lapauw, J. Halim, J. Lu, T. Cabioch, L. Hultman, M. Barsoum, K. Lambrinou, J. Vleugels, Synthesis of the novel Zr_3AlC_2 MAX phase, *Journal of the European Ceramic Society* 36 (3) (2016) 943–947.
- [20] T. Lapauw, K. Lambrinou, T. Cabioch, J. Halim, J. Lu, A. Pesach, O. Rivin, O. Ozeri, E. N. Caspi, L. Hultman, et al., Synthesis of the new MAX phase Zr_2AlC , *Journal of the European Ceramic Society* 36 (8) (2016) 1847–1853.
- [21] J. Xu, M.-Q. Zhao, Y. Wang, W. Yao, C. Chen, B. Anasori, A. Sarycheva, C. E. Ren, T. Mathis, L. Gomes, L. Zhenghua, Y. Gogotsi, Demonstration of Li-ion capacity of MAX phases, *ACS Energy Letters* 1 (6) (2016) 1094–1099.
- [22] H. Lin, Y. Chen, J. Shi, Insights into 2D MXenes for versatile biomedical applications: current advances and challenges ahead, *Advanced Science* 5 (10) (2018) 1800518.
- [23] H. Tong, S. Lin, Y. Huang, P. Tong, W. Song, Y. Sun, Difference in physical properties of MAX-phase compounds Cr_2GaC and Cr_2GaN induced by an anomalous structure change in Cr_2GaN , *Intermetallics* 105 (2019) 39–43.
- [24] Q. Tao, J. Lu, M. Dahlqvist, A. Mockute, S. Calder, A. Petruhins, R. Meshkian, O. Rivin, D. Potashnikov, E. N. Caspi, H. Shaked, A. Hoser, C. Opagiste, R.-M. Galera, R. Salikhov, U. Wiedwald, C. Ritter, A. R. Wildes, B. Johansson, L. Hultman,

- M. Farle, M. W. Barsoum, J. Rosén, Atomically layered and ordered rare-earth i-MAX phases: a new class of magnetic quaternary compounds, *Chemistry of Materials* 31 (7) (2019) 2476–2485.
- [25] L. Naslund, P. O. Persson, J. Rosén, X-ray photoelectron spectroscopy of Ti_3AlC_2 , $Ti_3C_2T_z$, and TiC provides evidence for the electrostatic interaction between laminated layers in MAX-Phase materials, *The Journal of Physical Chemistry C* 124 (50) (2020) 27732–27742.
- [26] M. Sanna, S. Ng, J. V. Vaghasiya, M. Pumera, Fluorinated MAX Phases for Photoelectrochemical Hydrogen Evolution, *ACS Sustainable Chemistry & Engineering* 10 (8) (2022) 2793–2801.
- [27] H. Shao, S. Luo, A. Descamps-Mandine, K. Ge, Z. Lin, P.-L. Taberna, Y. Gogotsi, P. Simon, Synthesis of MAX Phase Nanofibers and Nanoflakes and the Resulting MXenes, *Advanced Science* 10 (1) (2023) 2205509.
- [28] X.-H. Zha, X. Ma, S. Du, R.-Q. Zhang, R. Tao, J.-T. Luo, C. Fu, Role of the A-element in the structural, mechanical, and electronic properties of Ti_3AC_2 MAX phases, *Inorganic Chemistry* 61 (4) (2021) 2129–2140.
- [29] M. A. Saeed, A. Shahzad, K. Rasool, F. Mateen, J.-M. Oh, J. W. Shim, 2D MXene: a potential candidate for photovoltaic cells? A critical review, *Advanced Science* 9 (10) (2022) 2104743.
- [30] L. Chen, Y. Li, B. Zhao, S. Liu, H. Zhang, K. Chen, M. Li, S. Du, F. Xiu, R. Che, et al., Multiprincipal Element M_2FeC ($M = Ti, V, Nb, Ta, Zr$) MAX Phases with Synergistic Effect of Dielectric and Magnetic Loss, *Advanced Science* (2023) 2206877.
- [31] D. J. Tallman, E. N. Hoffman, E. N. Caspi, B. L. Garcia-Diaz, G. Kohse, R. L. Sindelar, M. W. Barsoum, Effect of neutron irradiation on select MAX phases, *Acta Materialia* 85 (2015) 132–143.
- [32] C. Ang, C. Silva, C. Shih, T. Koyanagi, Y. Katoh, S. J. Zinkle, Anisotropic swelling and microcracking of neutron irradiated Ti_3AlC_2 – $Ti_5Al_2C_3$ materials, *Scripta Materialia* 114 (2016) 74–78.
- [33] D. J. Tallman, L. He, B. L. Garcia-Diaz, E. N. Hoffman, G. Kohse, R. L. Sindelar, M. W. Barsoum, Effect of neutron irradiation on defect evolution in Ti_3SiC_2 and Ti_2AlC , *Journal of Nuclear Materials* 468 (2016) 194–206.
- [34] C. Ang, C. M. Parish, C. Shih, C. Silva, Y. Katoh, Microstructure and mechanical properties of titanium aluminum carbides neutron irradiated at 400–700°C, *Journal of the European Ceramic Society* 37 (6) (2017) 2353–2363.
- [35] D. J. Tallman, L. He, J. Gan, E. N. Caspi, E. N. Hoffman, M. W. Barsoum, Effects of neutron irradiation of Ti_3SiC_2 and Ti_3AlC_2 in the 121–1085°C temperature range, *Journal of Nuclear Materials* 484 (2017) 120–134.
- [36] M. A. Tunes, R. W. Harrison, S. E. Donnelly, P. D. Edmondson, A transmission electron microscopy study of the neutron-irradiation response of Ti-based MAX phases at high temperatures, *Acta Materialia* 169 (2019) 237–247.
- [37] T. Lapauw, B. Tunca, J. Joris, A. Jianu, R. Fetzer, A. Weisenburger, J. Vleugels, K. Lambrinou, Interaction of $M_{n+1}AX_n$ phases with oxygen-poor, static and fast-flowing liquid lead-bismuth eutectic, *Journal of Nuclear Materials* 520 (2019) 258–272.
- [38] D. Bowden, J. Ward, S. Middleburgh, S. de Moraes Shubeita, E. Zapata-Solvas, T. Lapauw, J. Vleugels, K. Lambrinou, W. Lee, M. Preuss, et al., The stability of irradiation-induced defects in Zr_3AlC_2 , Nb_4AlC_3 and $(Zr_{0.5}, Ti_{0.5})_3AlC_2$ MAX phase-based ceramics, *Acta Materialia* 183 (2020) 24–35.
- [39] B. Tunca, T. Lapauw, C. Callaert, J. Hadermann, R. Delville, E. N. Caspi, M. Dahlqvist, J. Rosén, A. Marshal, K. G. Pradeep, et al., Compatibility of Zr_2AlC MAX phase-based ceramics with oxygen-poor, static liquid lead–bismuth eutectic, *Corrosion Science* 171 (2020) 108704.
- [40] M. A. Tunes, M. Imtyazuddin, C. Kainz, S. Pogatscher, V. M. Vishnyakov, Deviating from the pure MAX phase concept: Radiation-tolerant nanostructured dual-phase Cr_2AlC , *Science advances* 7 (13) (2021) eabf6771.
- [41] M. A. Tunes, S. M. Drewry, J. D. Arregui-Mena, S. Picak, G. Greaves, L. B. Cattini, S. Pogatscher, J. A. Valdez, S. Fensin, O. El-Atwani, S. E. Donnelly, T. A. Saleh, P. D. Edmondson, Accelerated radiation tolerance testing of Ti-based MAX phases, *Materials Today Energy* (2022) 101186.
- [42] B. Tunca, G. Greaves, J. Hinks, P. O. Persson, J. Vleugels, K. Lambrinou, In situ He+ irradiation of the double solid solution $(Ti_{0.5}, Zr_{0.5})_2(Al_{0.5}, Sn_{0.5})C$ MAX phase: Defect evolution in the 350–800°C temperature range, *Acta Materialia* 206 (2021) 116606.
- [43] E. Gladyshevskii, Y. B. Kuz'ma, P. Kripyakevich, The crystal structures of Mn_3Ni_2Si , V_3Ni_2Si , Nb_3Ni_2Si and related Cr and Ta compounds, *Journal of Structural Chemistry* 4 (3) (1964) 343–355.
- [44] V. O. dos Santos, H. M. Petrilli, C. G. Schön, L. T. Eleno, Thermodynamic modelling of the Nb–Ni–Si phase diagram based on the 1073 K isothermal section using ab initio calculations, *Calphad* 51 (2015) 57–66.
- [45] V. O. dos Santos, M. A. Tunes, L. T. Eleno, C. G. Schön, K. W. Richter, Experimental investigation of phase equilibria in

the Nb–Ni–Si refractory alloy system at 1073 K, *Scripta Materialia* 164 (2019) 96–100.

- [46] V. O. dos Santos, L. T. Eleno, C. G. Schön, K. W. Richter, Experimental investigation of phase equilibria in the Nb–Ni–Si refractory alloy system at 1323 K, *Journal of Alloys and Compounds* 842 (2020) 155373.
- [47] M. Hellenbrandt, The inorganic crystal structure database (ICSD)—present and future, *Crystallography Reviews* 10 (1) (2004) 17–22.
- [48] D. A. Porter, K. E. Easterling, *Phase transformations in metals and alloys* (revised reprint), CRC press, 2009.
- [49] S. Coulombe, J.-L. Meunier, Theoretical prediction of non-thermionic arc cathode erosion rate including both vaporization and melting of the surface, *Plasma Sources Science and Technology* 9 (3) (2000) 239.
- [50] R. Radhakrishnan, J. Williams, M. Akinc, Synthesis and high-temperature stability of Ti_3SiC_2 , *Journal of Alloys and Compounds* 285 (1-2) (1999) 85–88.
- [51] N. Goossens, T. Lapauw, K. Lambrinou, J. Vleugels, Synthesis of MAX phase-based ceramics from early transition metal hydride powders, *Journal of the European Ceramic Society* 42 (16) (2022) 7389–7402.
- [52] D. C. Palmer, Visualization and analysis of crystal structures using CrystalMaker software, *Zeitschrift für Kristallographie-Crystalline Materials* 230 (9-10) (2015) 559–572.
- [53] K. Kuo, C. Dong, D. Zhou, Y. Guo, Z. Hei, D. Li, A Friauf-Laves (Frank-Kasper) phase related quasicrystal in a rapidly solidified Mn_3Ni_2Si alloy, *Scripta Metallurgica* 20 (12) (1986) 1695–1698.
- [54] M. Kolenda, A. Szytula, J. Leciejewicz, A. Pawlukojc, H. Ptasiwicz-Bak, Magnetic structure of Mn_3Ni_2Si , *Journal of Magnetism and Magnetic Materials* 89 (1-2) (1990) 26–28.
- [55] C. Wang, L. Huang, M. Yang, X. Huang, J. Zhang, S. Pan, S. Yang, X. Liu, Experimental investigation of phase equilibria in the Ni–Ta–Si refractory alloy system, *Journal of Alloys and Compounds* 888 (2021) 161467.
- [56] Y. B. Kuz'ma, E. Gladyshevskii, D. Byk, Crystal structure of some ternary compounds in the Nb–Co–Si system, *Journal of Structural Chemistry* 5 (4) (1964) 518–522.
- [57] N. Pavlyuk, G. Dmytriv, V. Pavlyuk, B. Rozdzynska-Kielbik, G. Cichowicz, M. K. Cyranski, I. Chumak, H. Ehrenberg, New cubic cluster phases in the Mg–Ni–Ga system, *Acta Crystallographica Section B: Structural Science, Crystal Engineering and Materials* 76 (4) (2020) 534–542.
- [58] M. Radovic, M. W. Barsoum, MAX phases: bridging the gap between metals and ceramics, *American Ceramics Society Bulletin* 92 (3) (2013) 20–27.
- [59] A. Jain, S. P. Ong, G. Hautier, W. Chen, W. D. Richards, S. Dacek, S. Cholia, D. Gunter, D. Skinner, G. Ceder, Commentary: The Materials Project: A materials genome approach to accelerating materials innovation, *APL Materials* 1 (1) (2013) 011002.
- [60] S. Sun, Y. Yu, S. Sun, Q. Wang, T. Chen, J. Chen, Y. Zhang, W. Cui, Magnetic properties and microstructures of Fe-doped $(Ti_{1-x}Fe_x)_3AlC_2$ MAX phase and their mxene derivatives, *Journal of Superconductivity and Novel Magnetism* 34 (2021) 1477–1483.
- [61] Y. Li, J. Liang, H. Ding, J. Lu, X. Mu, P. Yan, X. Zhang, K. Chen, M. Li, P. O. Persson, et al., Near-room temperature ferromagnetic behavior of single-atom-thick 2D iron in nanolaminated ternary MAX phases, *Applied Physics Reviews B* 8 (3) (2021) 031418.
- [62] G. Deysheer, C. E. Shuck, K. Hantanasirisakul, N. C. Frey, A. C. Foucher, K. Maleski, A. Sarycheva, V. B. Shenoy, E. A. Stach, B. Anasori, et al., Synthesis of Mo_4VAIC_4 MAX phase and two-dimensional Mo_4VC_4 MXene with five atomic layers of transition metals, *ACS Nano* 14 (1) (2019) 204–217.
- [63] T. Lapauw, B. Tunca, T. Cabioc'h, J. Lu, P. O. Persson, K. Lambrinou, J. Vleugels, Synthesis of MAX phases in the Hf–Al–C system, *Inorganic Chemistry* 55 (21) (2016) 10922–10927.
- [64] B. Tunca, T. Lapauw, R. Delville, D. R. Neuville, L. Hennet, D. Thiaudière, T. Ouisse, J. Hadermann, J. Vleugels, K. Lambrinou, Synthesis and characterization of double solid solution $(Zr,Ti)_2(Al,Sn)C$ MAX phase ceramics, *Inorganic Chemistry* 58 (10) (2019) 6669–6683.
- [65] T. Lapauw, B. Tunca, D. Potashnikov, A. Pesach, O. Ozeri, J. Vleugels, K. Lambrinou, The double solid solution $(Zr,Nb)_2(Al,Sn)C$ MAX phase: a steric stability approach, *Scientific reports* 8 (1) (2018) 12801.
- [66] L. A. Giannuzzi, F. A. Stevie, A review of focused ion beam milling techniques for TEM specimen preparation, *Micron* 30 (3) (1999) 197–204.
- [67] G. Cliff, G. Lorimer, Quantitative analysis of thin metal foils using EMMA-4, the ratio technique, in: *Proceedings of the*

5th European Congress on Electron Microscopy, The Institute of Physics, London, 1972, pp. 140–141.

[68] G. Cliff, G. W. Lorimer, The quantitative analysis of thin specimens, *Journal of Microscopy* 103 (2) (1975) 203–207.

[69] B. Sundman, B. Jansson, J.-O. Andersson, The thermo-calc databank system, *Calphad* 9 (2) (1985) 153–190.

[70] K. Momma, F. Izumi, Vesta 3 for three-dimensional visualization of crystal, volumetric and morphology data, *Journal of applied crystallography* 44 (6) (2011) 1272–1276.